Modeling of high temperature direct methanol solid oxide fuel cells

Qidong Xu[a], Meng Ni[a*]

[a] *Building Energy Research Group, Department of Building and Real Estate, The Hong Kong Polytechnic University, Hung Hom, Kowloon, Hong Kong, China*

Summary:

Methanol is a promising fuel for solid oxide fuel cells (SOFCs). A 2D numerical model is developed to study a tubular direct methanol SOFC. The model fully considers the methanol decomposition reaction (MDR) and water gas shift reaction (WGSR) in the anode, the electrochemical oxidations of H_2 and CO, fluid flow and mass transfer in the cell. The model is validated by the direct methanol SOFC experiment, which achieved a peak power density of 1.3 W cm^{-2} at 1073 K. Subsequent parametric simulations are conducted to understand the effects of operating and structural parameters on the SOFC performance, such as temperature, potential, anode thickness and cell length. It is found that the performance of direct methanol SOFC increases with increasing inlet temperature because of the enhanced chemical reaction rates, electrochemical reaction rates, as well as ionic conduction at a higher temperature. In addition, higher methanol conversion can be achieved by increasing the anode thickness and cell length. The current density is found to increase with slight increase in anode thickness but decrease with increasing SOFC length. The results form a basis for subsequent performance enhancement of direct methanol SOFC by optimization of the cell structure and operating parameters.

Keywords: solid oxide fuel cell; Methanol fuel; Modeling; Water gas shift reaction (WGSR); Direct internal reforming (DIR).

[*] Corresponding author (M. Ni)
Email: meng.ni@polyu.edu.hk; Tel: 852-27664152; Fax: 852-27645131

Nomenclature

Abbreviation

YSZ	Yttrium-stabilized zirconium
LSM	Lanthanum strontium manganate
SOFC	Solid oxide fuel cell
SCCM	Standard cubic centimeters per minute
TPB	Triple-phase boundary
MDR	Methanol decomposition reaction
WGSR	Water gas shift reaction

Roman

c	Total concentration of the gas mixture, mol m^{-3}
D_{ij}	Binary diffusion coefficient of *i* and *j*, $cm^2\ s^{-1}$
D_{ik}	Knudsen diffusion coefficient of *i*, $cm^2\ s^{-1}$
D_{ij}^{eff}	Effective binary diffusion coefficient of *i* and *j*, $cm^2\ s^{-1}$
E	Equilibrium Nernst potential, V
F	Faraday constant, 96,485 C mol^{-1}
i	Current density, A m^{-2}
i_0	Exchange current density, A m^{-2}
j_i	Mass diffusion flux of species *i*, kg $m^{-2}\ s^{-1}$
J_i	Molar diffusion flux of species *i*, mol $m^{-2}\ s^{-1}$
L_{cell}	Cell length, mm
M_i	Molecular weight of species *i*, kg mol^{-1}
n	Number of electrons transferred per electrochemical reaction
N_i	Molar flux of species *i*, mol $m^{-2}\ s^{-1}$
p	(partial) Pressure, Pa
Q_m	Mass source, kg
r	Mean pore radius, m
R	Gas constant, 8.3145 J $mol^{-1}\ K^{-1}$
R_r	Rate of chemical reaction, mol $m^{-3}\ s^{-1}$
R_i	Rate of generation or consumption of species *i*, mol $m^{-3}\ s^{-1}$
S	Specific surface area, $m^2\ m^{-3}$
T	Temperature, K
U	Mass-averaged velocity, m s^{-1}
u	Molar-averaged velocity, m s^{-1}
V	Volume fraction
y_i	Molar fraction of species *i*

Greek letters

α	Charge transfer coefficient
ε	Porosity
κ	Permeability, m^2
μ	Dynamic viscosity of gas mixture, Pa s
μ_i	Dynamic viscosity of species *i*, Pa s
η	Polarization, V
ρ	Mass concentration of the mixture, kg m^{-3}
σ	Electrical conductivity, S m^{-1}
τ	Tortuosity
ω_i	Mass fraction of species *i*

Subscripts

a	Anode
act	Activation
c	Cathode
i	Species *i*
l	Ionic phase
s	Electronic phase

Superscripts

eff	Effective
l	Local

1 Introduction

Solid Oxide Fuel Cells (SOFCs) are environmentally-friendly and efficient devices for converting the chemical energy of the reactants into the electric power via the electrochemical reactions.[1] As the ceramic electrolyte materials like YSZ (yttrium-stabilized zirconia) require a high temperature for fast O^{2-} conduction, SOFCs normally operate at 600 ° to 1000 ℃. The high operating temperature offers SOFCs various advantages over low temperature fuel cells like PEMFCs (proton exchange membrane fuel cells), such as the use of low-cost catalyst. In addition, CO is a poisonous gas for PEMFCs but could be considered as the fuel for electricity generation by an SOFC.[2] Although hydrogen is an ideal fuel for SOFC due to the fast oxidation kinetics, it is still challenging to produce and store hydrogen efficiently and economically. Compared with PEMFC, a distinct feature of SOFC is fuel flexibility. Various gaseous fuels, such as methane,[3,4] methanol,[5,6] ammonia,[7,8] etc., can be used as fuels by SOFCs for power generation due to the internal reforming of hydrocarbons or ammonia thermal decomposition in the SOFC anode. In addition, solid carbon even biomass can be used as fuel in SOFC[9,10].

Among various carbonaceous fuels, methanol is a promising fuel for SOFC due to a number of reasons. Methanol is the simplest alcohol and has a relatively higher H/C ratio of 4:1, which is same as methane.[9] Compared with methane fuel, the carbon deposition is not a big concern for SOFC since the oxygen atom in methanol does not favour the carbon deposition reaction. In addition, the transportation and storage of liquid methanol at ambient pressure and temperature is more convenient than those of gaseous fuels such as methane.[9] Besides, the volumetric energy density of methanol is almost up to 1.6×10^4 kJ m^{-3}, which is about half to that of gasoline, but much higher than that of liquid hydrogen.[10,11] Moreover, unlike other heavier alcohols like ethanol (C_2H_5OH) with the C-C bond in the molecular structures, the cleavage of C-H bonds is much easier for methanol through methanol thermal decomposition ($CH_3OH \rightarrow CO + 2H_2$) or steam reforming of methanol ($CH_3OH + H_2O \rightarrow CO_2 + 3H_2$).[9,12] Actually, methanol has been extensively studied as a promising fuel in other types of fuel cells such as the DMFC (Direct Methanol Fuel cell with a polymer electrolyte). However, lower current density (typically less than 100 mW cm^{-2},[13,14] because of the sluggish anode kinetics) and lower efficiency (due to the crossover of methanol from the anode side to the cathode side) limit the wide application of DMFC.[15,16] In addition to the polymer electrolyte based DMFC, the use of methanol in SOFC has been experimentally studied. Jiang et al.[17] fabricated an anode-supported SOFC with YSZ as the thin film electrolyte, and achieved high power densities of 0.6 W cm^{-2} at 923 K and 1.3 W cm^{-2} at 1073 K using pure methanol as a fuel.

Although there are no details of the long-term test for the carbon resistance, no noticeable carbon deposition was observed in the anode after experiments, which demonstrated the feasibility of the direct methanol SOFC without the coking issues. Liu et al.[18] developed an SOFC assembled by Ni/SDC-SDC-SSC/SDC (anode-electrolyte-cathode, SDC: Sm-doped ceria; SSC: $Sm_{0.5}Sr_{0.5}CoO_3$.). Using methanol fuel, the SOFC achieved the maximum power densities of 0.223, 0.43 and 0. 698 W cm^{-2} at 550, 600 and 650 ℃, respectively, which were only slightly lower than those using hydrogen fuel. After 160 h operation stability test, there is no degradation observed in the performance of the cell. Meng et al.[19] developed an anode-supported SOFC with the porous Ni/SDC anode, the SDC thin film electrolyte and the composite LSCF/SDC (LSCF: $La_{0.6}Sr_{0.4}Co_{0.2}Fe_{0.8}O_3$) cathode and achieved a peak power density of 0.82 W cm^{-2} at 600 ℃. EDX analysis showed that no coke formation in the cermet anode layer after the durability test over 60 h. Sasaki et al.[20] showed comparable performances of SOFC with Ni/YSZ composite anode using CH_3OH fuel and the H_2/CO mixture (with molar ratio of 2:1). Saunders et al. also demonstrated that the CH_3OH fueled SOFC performed comparably with the H_2 fueled SOFC.[21] According to the analyses of the above experimental researches, carbon deposition is thermodynamically unfavored due to the methanol's high oxygen to carbon ratio in the molecular structure. Therefore, coking issue could be partially or fully inhibited in the direct methanol SOFC under some operating conditions such as the higher temperature (thermodynamically), higher current density (more flux of the oxygen ions) and higher ion conductivity of the ceramic phase in the cermet anode.

The above-mentioned experimental studies demonstrated the feasibility of the high-performance direct methanol SOFC with the state-of-the-art Ni-based anode configuration. However, the present literature is lacking a detailed numerical modeling study on the complicated chemical and physical processes in the SOFC as the chemical reactions, electrochemical reactions, and transport processes are highly coupled. For example, the operating temperature may significantly affect the chemical reaction rates, which in turn may influence the gas composition of the cell and subsequently affect the fuel cell power output. A comprehensive understanding of these phenomena is essential for optimizing the operating conditions and the fuel cell micro- and macro-structures for performance enhancement. Therefore, in order to fill this research gap, a 2D comprehensive model for direct methanol SOFC is developed and parametric simulations are performed.

The 2D mathematic model fully considers the chemical reactions (methanol reforming reaction and water gas shift reaction), electrochemical reactions and mass transfer in a tubular SOFC running on CH_3OH fuel. The typical SOFC configuration of Ni/YSZ-YSZ-YSZ/LSM

is used. The modeling results are compared with the experimental results of Jiang et al.[17] for model validation. Detailed parametric simulations are conducted to investigate the mass transfer, fluid flow and internal reforming reaction with considering the electrochemical oxidations of both CO and H_2 in the anode. The effects of the operating conditions (inlet temperature and operating potential) and the structural parameters (length of the cell and thickness of the anode) on the performance of CH_3OH fueled SOFC are also investigated in detail.

2 Model development

2.1 Working mechanism and simulation assumptions

In the present study, a 2D numerical model is developed for the methanol fueled SOFC. The schematics of the anode-supported SOFC and the working mechanism are shown in Figure 1. According to the experimental set-up of Jiang et al.'s study,[17] the computational domain of the SOFC includes anode channel (fuel channel), Ni/YSZ porous anode, YSZ dense electrolyte, YSZ/LSM porous cathode, and cathode channel (air channel). In addition to gas transport through the porous electrodes, the chemical reactions also take place in the porous anode. The dense electrolyte is a gas-tight, oxygen-ion conducting layer which separates the gases of cathode and anode. The values of materials and specific dimensions of the SOFC are set to be consistent with the experimental set-up, as summarized in Table 1.

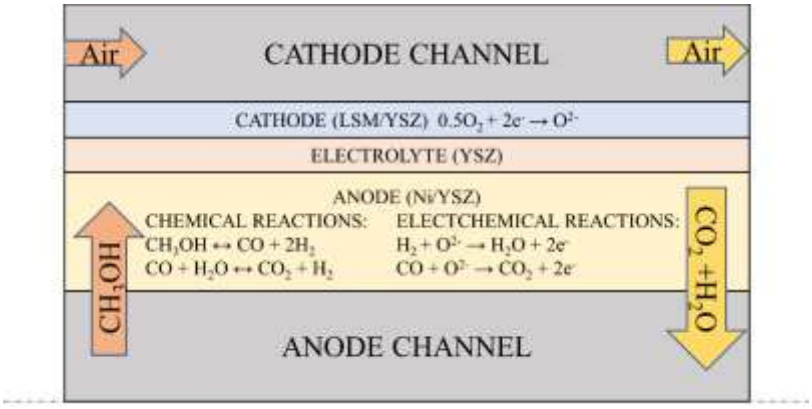

Figure 1 Schematic of the anode-supported SOFC operating on the pure methanol.

Table 1 Model parameters.[17,22,23]

Parameter	Value or expression	Unit
Ionic conductivity		
YSZ	$3.34 \times 10^4 \times e^{\frac{-10300}{T}}$	S m^{-1}
Electronic conductivity		
Ni	$3.27 \times 10^6 - 1065.3 \times T$	S m^{-1}
LSM	$4.2 \times 10^7 / T \times e^{\frac{-1150}{T}}$	S m^{-1}
Porosity		

Cathode	0.46	
Anode	0.46	
S_{TPB}		
Cathode layer	3.33×10^5	$m^2\ m^{-3}$
Anode layer	2.66×10^5	$m^2\ m^{-3}$
Tortuosity	3	
Anode-supported SOFC		
Cell length	9	mm
Ni-YSZ porous anode	1.02	mm
YSZ electrolyte	0.01	mm
LSM-YSZ cathode	0.1	mm

In operation, CH_3OH and air are supplied to the anode channel and cathode channel, respectively. CH_3OH is diffused from the anode channel into the porous anode, where with the Ni metal catalyst CH_3OH fuel is converted to CO and H_2 through the methanol decomposition reaction (MDR, Equation 1).[9,24] Due to the generation of the steam by the electrochemical oxidation of the hydrogen (Equation 3), water gas shift reaction (WGSR, Equation 2) will take place to produce CO_2 and more H_2 in the anode catalyst layer.

$$CH_3OH \leftrightarrow CO + 2H_2 \quad (1)$$

$$CO + H_2O \leftrightarrow CO_2 + H_2 \quad (2)$$

At the triple phase boundary (TPB) of the porous anode, both H_2 and CO can be electrochemically oxidized by O^{2-} to produce electrons and H_2O or CO_2 (Equations 3 and 4). The electrons are subsequently collected by the current collector and transported via the external circuit to the cathode, where electrons react with O_2 molecules to form O^{2-} (Equation 5), followed by O^{2-}transport from the cathode to the anode via the dense electrolyte. Therefore, as long as the fuel and air are supplied to the anode and cathode, the electrical power can be generated continuously.

$$H_2 + O^{2-} \rightarrow H_2O + 2e^- \quad (3)$$

$$CO + O^{2-} \rightarrow CO_2 + 2e^- \quad (4)$$

$$0.5O_2 + 2e^- \rightarrow O^{2-} \quad (5)$$

In this study, only MDR and WGSR reactions are considered to be the possible chemical reactions in the porous anode. The methanation reaction ($CO + 3H_2 \leftrightarrow CH_4 + H_2O$) requires a high pressure and a relatively lower temperature, which is not favoured under the fuel cell operation condition.[24] Although the Boudouard reaction ($2CO \leftrightarrow CO_2 + C$) is also thermodynamically unfavoured in the SOFC because of the exothermic nature of the reaction,[24] it should be noticed that the carbon may deposit on the anode catalyst surface due to the faster kinetics of the Boudouard reaction caused by the high temperature in the cell, and the carbon

deposition is detrimental to the performance of SOFCs by blocking the pores, covering the TPB, and even destroying the anode structure (under extreme conditions).[25] Boudouard reaction is assumed to be negligible in the present work as the O atom in CH_3OH does not favour the formation of C, in comparison with the CH_4 fuel. This assumption is also consistent with experimental results without any noticeable carbon deposition.[17-21] However, it should be noted that the other chemical reactions may become significant under certain conditions. For example, carbon deposition may happen under certain temperature and current densities. They can be considered in the subsequent studies when more reliable data are available.

Based on the principles of the SOFC running on the pure methanol, the main assumptions used in simulations are presented below.

(1) Only H_2 and CO can be electrochemically oxidized due to their relatively high reaction kinetics;
(2) The catalyst sites for electrochemical oxidations of H_2 as well as CO and the electrochemical reduction of the O_2 are uniformly distributed in the porous anode and cathode, respectively;
(3) In addition, the electron conduction in the electrodes and the oxygen ion (O^{2-}) transport in the anode-electrolyte-cathode are assumed to be homogeneous and continuous;
(4) All gases are treated as ideal gases, which obey the ideal gas law ($PV = nRT$), and the dynamic viscosity of the ideal gas species is independent of the pressure;
(5) The temperature distribution is considered to be uniform within the whole cell due to the small cell size, and all parameters are calculated at the given constant temperature;
(6) The fluid flow in the SOFC is considered as the laminar flow due to relatively lower Reynolds number.

2.2 Governing equations

The mathematic model mainly includes the following sub-models: chemical reaction model, electrochemical reaction model, and computational fluid dynamics (CFD) model as well as the mass transfer model.

2.2.1 Chemical reaction model

The chemical reaction model is developed to compute the chemical reactions rates and the species source terms for the mass transfer model involved in processes of the cell. Both MDR (Equation 1) and the reversible WGSR (Equation 2) are considered for the SOFC anode. The reaction rates for MDR (R_{MDR}, mol m^{-3} s^{-1}) and reversible WGSR (R_{WGSR}, mol m^{-3} s^{-1}) can be calculated below:

The MDR[26] :

$$R_{MDR} = k_D P_{CH_3OH} E_{qD} \quad (6)$$

$$E_{qD} = 1 - \frac{P_{CO} p_{H_2}^2}{K_{eq,D} P_{CH_3OH}} \quad (7)$$

$$K_{eq,D} = 1.718 \times 10^{14} \exp\left(-\frac{95419}{RT}\right) \quad (8)$$

The WGSR[27] :

$$R_{WGSR} = k_{sf}\left(P_{H_2O} P_{CO} - \frac{P_{H_2} P_{CO_2}}{K_{ps}}\right) \quad (9)$$

$$k_{sf} = 0.0171 \exp\left(-\frac{103191}{RT}\right) \quad (10)$$

$$K_{ps} = \exp\left(-0.2935Z^3 + 0.6351Z^2 + 4.1788Z + 0.3169\right) \quad (11)$$

$$Z = \frac{1000}{T(K)} - 1 \quad (12)$$

where the k_D is the tuning parameter for the model validation. It should be noted that these reactions are considered negligible in the fuel channel because of the lack of the catalyst.[28]

2.2.2 Electrochemical reaction model

The output current density (i, A m^{-2}) can be calculated at the specific operating potential by the electrochemical reaction model. It is known that current density is related to the electrochemical reaction rate, and in electrochemistry, the Butler-Volmer (BV) equation is a fundamental function for linking the current density with the activation overpotential (η_{act}, V). In this study, the current density generated from the electrochemical reactions (Equations 3, 4 and 5) can be calculated from:

$$i = i_0 \left\{\exp\left(\frac{\alpha n F \eta_{act}}{RT}\right) - \exp\left(\frac{-(1-\alpha) n F \eta_{act}}{RT}\right)\right\} \quad (13)$$

where i_0 is the exchange current density. From the literature, the i_0 for H_2 and O_2 are set to be 5300 A m^{-2} and 2000 A m^{-2}, respectively.[28] Besides, the electrochemical oxidation reaction rate of the CO is about 0.32-0.52 times that of the H_2 at about 800 °C,[29] and considering the advancement of the electrode activity for the CO oxidation. Therefore, i_0 for CO in the present work is set to be 3000 A m^{-2}.[28] n is the number of the electrons released from the per electrochemical reaction; F is the Faraday constant (96,485 C mol^{-1}); R is the universal gas constant (8.3145 J mol^{-1} K^{-1}); T (K) is the temperature. The activation overpotential (η_{act}) can be calculated as:

$$V = E - \eta_{act,a} - \eta_{act,c} - \eta_{ohmic} \quad (14)$$

Here η_{ohmic} (V) is the ohmic loss caused by the transport of the electrons and the ions; E (V) is thermodynamic equilibrium potential (Nernst potential), and equilibrium potentials for H_2 and CO can be expressed respectively by the Nernst equations[28] :

$$E_{H_2} = E_{H_2}^T + \frac{RT}{2F}\left[\frac{p_{H_2}^l \left(p_{O_2}^l\right)^{0.5}}{p_{H_2O}^l}\right] \quad (15)$$

$$E_{CO} = E_{CO}^T + \frac{RT}{2F}\left[\frac{p_{CO}^l \left(p_{O_2}^l\right)^{0.5}}{p_{CO_2}^l}\right] \quad (16)$$

where p_i^l (Pa) is the local partial pressure of species i; $E_{H_2}^T$ and E_{CO}^T are the equilibrium potentials at the pressure of 1 atm (101,325 Pa), which follow a linear relationship with the temperature[28] :

$$E_{H_2}^T = 1.253 - 0.00024516T \quad (17)$$

$$E_{CO}^T = 1.46713 - 0.0004527T \quad (18)$$

It should be noticed that the calculation of equilibrium potentials in the Nernst equations (Equations 15 and 16) is based on the local gas partial pressures at the triple phase boundary, so the concentration potential losses are theoretically included in the equilibrium potentials calculation.

The ohmic overpotential (η_{ohmic}) can be described by the Ohm's law, from which, the electronic/ionic phase potential can be calculated as:

$$i_l = -\sigma_l^{eff} \nabla(\emptyset_l) \quad (19)$$

$$i_s = -\sigma_s^{eff} \nabla(\emptyset_s) \quad (20)$$

where $\emptyset_l$ and $\emptyset_s$ (V) are the potentials of ion-conducting phase and electron-conducting phase, respectively; σ_l^{eff} and σ_s^{eff} (S m^{-1}) are the effective ionic conductivity and electronic conductivity of the electrodes. The effective conductivities can be calculated by the material intrinsic conductivity with the correction of microstructures of the porous electrodes:

$$\sigma_l^{eff} = \sigma_l \cdot \frac{V_l}{\tau_l} \quad (21)$$

$$\sigma_s^{eff} = \sigma_s \cdot \frac{V_s}{\tau_s} \quad (22)$$

here V represents the volume fraction in the electrodes and the τ is the tortuosity.[23]

2.2.3 CFD model

The CFD model is developed to simulate the fluid flow in the electrodes and the channels. Fluid flow is governed by the conservations of the mass and the momentum. In the gas channels, the typical Navier–Stokes equations of the steady state are applied:

Mass conservation:

$$\rho \nabla \cdot U = 0 \quad (23)$$

Momentum conservation:

$$\rho(U \cdot \nabla) \cdot U = -\nabla p + \nabla \cdot [\mu(\nabla U + \nabla U^T)] \quad (24)$$

Since the mass and momentum in the electrodes will change because of the electrochemical reactions, the extension of the Navier–Stokes equations, the Brinkman equations, are employed to describe the fluid velocity and the pressure field in the porous media, which extend Darcy' law to account for the dissipation of the kinetic energy by the viscous shear, as shown below:

Mass conservation:

$$\rho \nabla \cdot U = Q_m \tag{25}$$

Momentum conservation:

$$\frac{1}{\varepsilon}\rho(U \cdot \nabla) \cdot U\frac{1}{\varepsilon} = -\nabla p + \nabla \cdot \left[\mu\frac{1}{\varepsilon}(\nabla U + \nabla U^T) - \frac{2}{3}\mu\frac{1}{\varepsilon}(\nabla \cdot U)\right] - \left(\mu\kappa^{-1} + \frac{Q_m}{\varepsilon^2}\right)U \tag{26}$$

where ε and κ (m^2) are the porosity and the permeability of the electrodes; p and U (m s^{-1}) represent the pressure and velocity, respectively; Q_m (kg) is the amount of the mass change due to the electrochemical reactions; μ (Pa s) is the dynamic viscosity of the gas mixture, which can be expressed by:

$$\mu = \sum_{i=1}^{n} \frac{y_i \mu_i}{\sum_{j=1}^{n}\left(y_i \sqrt{\frac{M_j}{M_i}}\right)} \tag{27}$$

where y_i, μ_i and M_i (kg mol^{-1}) are the molar fraction, dynamic viscosity and molecular weight of species i, respectively. The dynamic viscosities for the gases are summarized in Table 2.

Table 2 Dynamic viscosities of the gases.[30]

μ_i	Value	Unit
CO	$(23.811 + 0.53944 \times T - 1.5411 \times 10^{-4} \times T^2) \times 10^{-7}$	Pa s
CO_2	$(11.811 + 0.49838 \times T - 1.0851 \times 10^{-4} \times T^2) \times 10^{-7}$	Pa s
H_2	$(27.758 + 0.212 \times T - 3.28 \times 10^{-5} \times T^2) \times 10^{-7}$	Pa s
H_2O	$(-36.826 + 0.429 \times T - 1.62 \times 10^{-5} \times T^2) \times 10^{-7}$	Pa s
CH_3OH	$(-14.236 + 0.38935 \times T - 6.2762 \times 10^{-5} \times T^2) \times 10^{-7}$	Pa s

2.2.4 Mass transfer model

The SOFC is a multicomponent system, and the concentrations of different species (uncharged species) in different regions are in general different. In order to determine the gas composition within the whole SOFC (except the dense electrolyte), the mass transfer model is used since it deals with the situations involving electrochemical/chemical reactions, fluid convection and diffusion or mixing phenomena. Therefore, the differential molar balance equations of component i are given by:

In the gas channels:

$$c\frac{\partial y_i}{\partial t} + \nabla \cdot J_i + c(u \cdot \nabla)y_i = 0 \tag{28}$$

In the electrodes:

$$\varepsilon \cdot c\frac{\partial y_i}{\partial t} + \nabla \cdot J_i + c(u \cdot \nabla)y_i = R_i \quad (29)$$

where J_i (mol m^{-2} s^{-1}) is the molar diffusion flux of species i; c (mol m^{-3}) is the total concentration of the gas mixture, and R_i (mol m^{-3} s^{-1}) represents the rate of generation or consumption of species i due to the homogeneous chemical reactions or the electrochemical reactions inside the porous electrodes; u (m s^{-1}) denotes the molar average velocity of the mixture, which is different from the mass average velocity U dealt with in Navier–Stokes equations. For the steady state system, the first terms on the left-hand sides of the Equations 28 and 29 equal 0.

Stefan-Maxwell model is used to calculate the diffusion flux of species i.[31] In the free channel, the molecular diffusion or continuum diffusion dominates,[32] while in the porous media, diffusion is an intermediate state between molecular diffusion and Knudsen diffusion.[33] Therefore, the diffusion model of the steady state is given by:

In the gas channels:

$$\sum_{j=1,j\neq i}^{n} \frac{y_j N_i - y_i N_j}{D_{ij}} = -c\frac{dy_i}{dx} \quad (30)$$

In the electrodes:

$$\sum_{j=1,j\neq i}^{n} \frac{y_j N_i - y_i N_j}{D_{ij}^{eff}} = -c\frac{dy_i}{dx} \quad (31)$$

here N_i (mol m^{-2} s^{-1}) is the molar flux of species i; D_{ij} (m^2 s^{-1}) denotes the binary diffusion coefficient of species i and j; D_{ij}^{eff} (m^2 s^{-1}) is the effective binary diffusion coefficient of species i and j, which is determined by the molecular diffusion coefficient and the Knudsen diffusion coefficient as well as the microstructures of the porous electrodes[34] :

$$D_{ij}^{eff} = \frac{\varepsilon}{\tau}\left(\frac{1}{D_{ij}} + \frac{1}{D_{ik}}\right)^{-1} \quad (32)$$

From the kinetic theory,[35] the Knudsen diffusion coefficient (D_{ik}) is govern by:

$$D_{ik} = \frac{2}{3} r\sqrt{\frac{8RT}{\pi M_i}} \quad (33)$$

where r (m) is the mean pore radius.

2.3 Numerical methods and validation

The governing equations of the model are solved by the Finite Element Method using the commercial software COMSOL 5.4. The computation domain is discretized into 52,000 elements to ensure the grid-independence of the results. The preliminary simulation results are compared with the experimental data with good as shown in Figure 2, and the average error in terms of the deviation between simulation and experimental data at 1073 K is 6.05% , which

validates the present model. The operating conditions and tuning parameter for the validation are summarized in Table 3. Same parameters (except typical operating conditions and structural dimensions) are used for the subsequent parametric simulations.

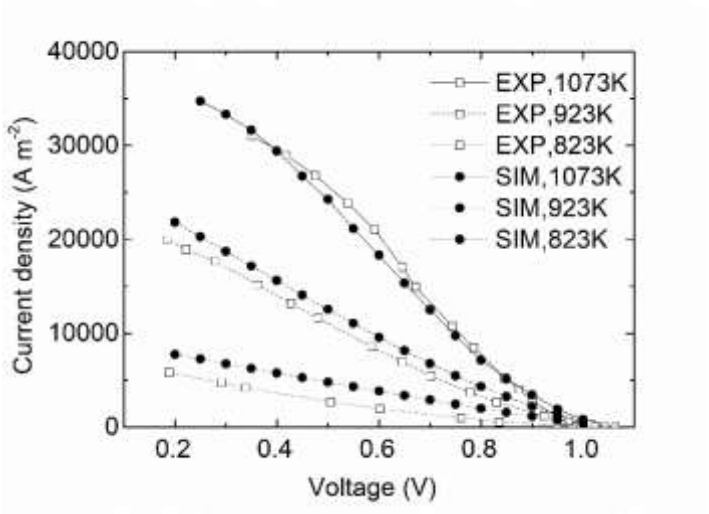

Figure 2 Model validation for the methanol-fueled SOFC at 1073 K, 923 K and 823 K.

Table 3 Operation parameters for model validation.

Parameters	Value	Unit
Anode inlet fuel flow rate (liquid)	0.2	ml min^{-1} (std)
Cathode inlet gas flow rate/velocity	600/1.13(1073 K)	SCCM/m s^{-1}
Anode inlet gas composition	CH_3OH (100%)	
Cathode inlet gas composition	O_2 (21%) + N_2 (79%)	
Operating temperature	1073, 923, 873	K
Operating pressure	1	atm
Operating potential	0.2 - 1.0	V
H_2 exchange current density	5300	A m^{-2}
CO exchange current density	3000	A m^{-2}
O_2 exchange current density	2000	A m^{-2}
Equilibrium constant of methanol decomposition reaction, k_D	0.004	

3 Results and discussion

3.1 Base case

Figure 3 shows the distributions of rates of chemical reactions and the molar fractions of species at an inlet temperature of 1073 K, and operating potential of 0.6 V. It is found that the rate of MDR is the highest (405 mol m^{-3} s^{-1}) at the inlet near the gas channel and decreases significantly along the anode layer (Figure 3a), which is mainly caused by the lower concentration of CH_3OH in the downstream of the anode (Figure 3b). Because of the high MDR rate, the molar fraction of CH_3OH decreases considerably along the gas channel. Besides, the rate distribution of WGSR is totally different from that of MDR. For the WGSR, the rate is

highest (15.2 mol m^{-3} s^{-1}) at the outlet near the electrolyte and increases along the anode (Figure 3c), which is because of the high concentration of the reactant (H_2O) near the interface of electrolyte and anode in the downstream (Figure 3d). High molar fraction of the water near the outlet in the porous anode is mainly due to the gas transport and the electrochemical reaction:

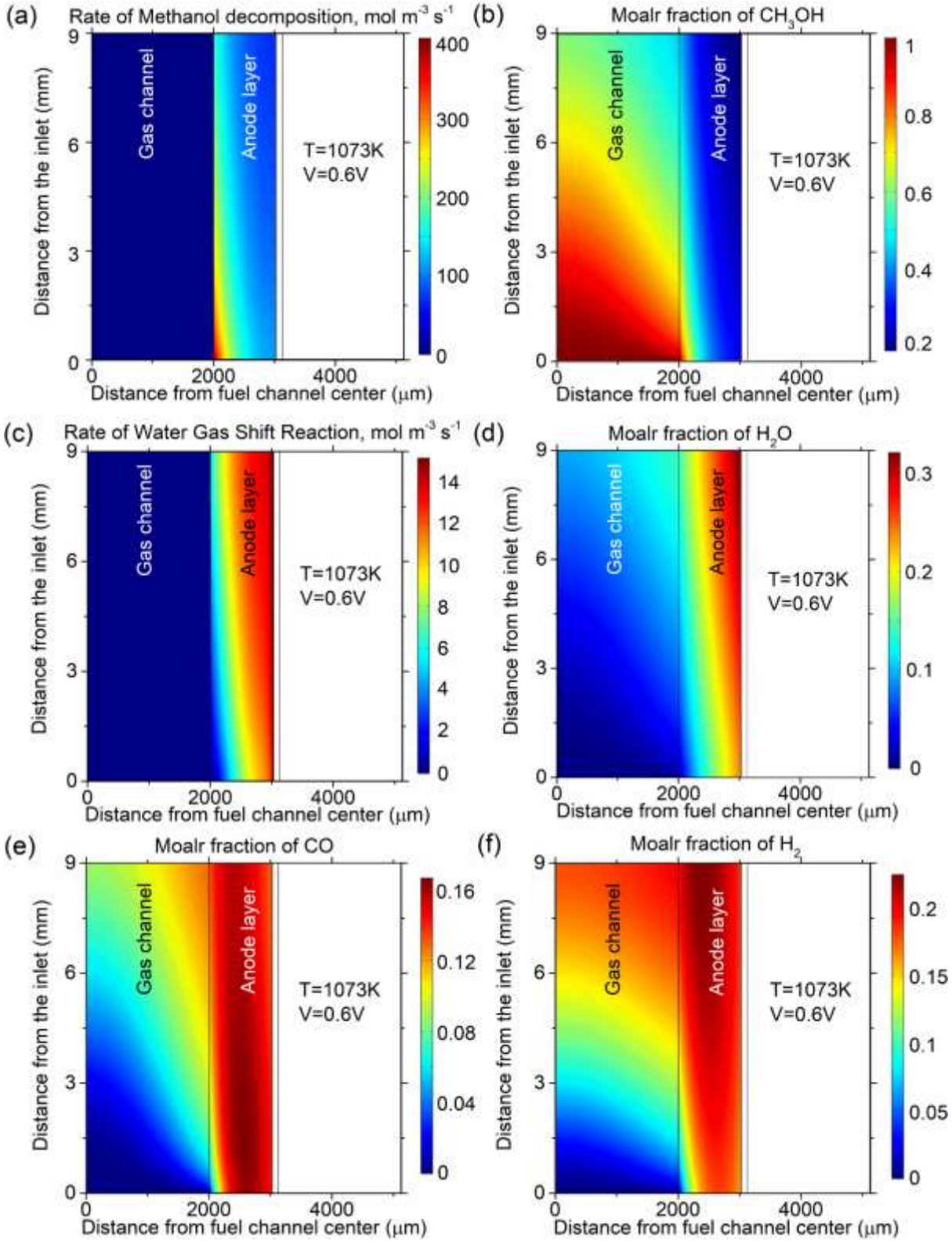

Figure 3 Reaction rate distributions and species molar fractions at 1073 K, 0.6 V: (a) MDR;

(b) CH_3OH; (c) WGSR; (d) H_2O; (e) CO; (f) H_2.

high electrochemical reaction rate (high current density) at TPB consuming more H_2 and producing more H_2O, and slow diffusion leading to the accumulation of the H_2O in the anode layer, thus cause huge concentration gradient between the gas channel and the porous anode.

It can be observed that the higher molar fraction of CO near the inlet (Figure 3e) is mainly due to the locally higher rate of MDR (producing more CO) and lower rate of WGSR (consuming less CO), as shown in Figure 3a and Figure 3c. For comparison, the molar fraction of H_2 shows an opposite trend and H_2 almost accumulates near the outlet (Figure 3f), which is due to the locally higher rate of WGSR (producing more H_2), as evidenced by the species fraction distribution in Figure 4.

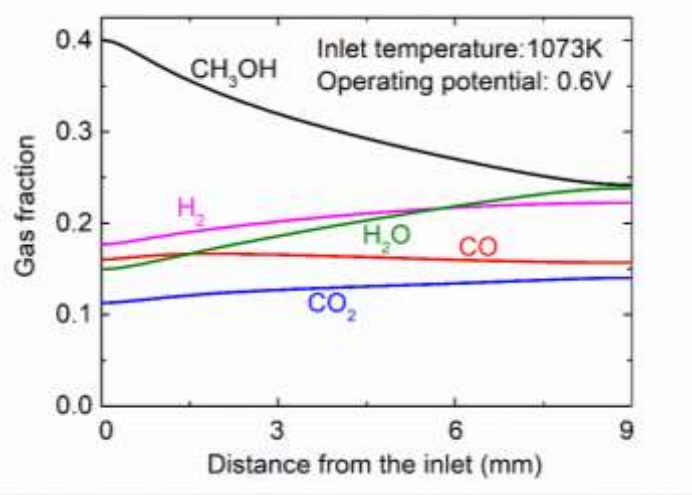

Figure 4 Gas composition at the center of porous anode at 1073 K, 0.6 V.

3.2 The effect of the temperature

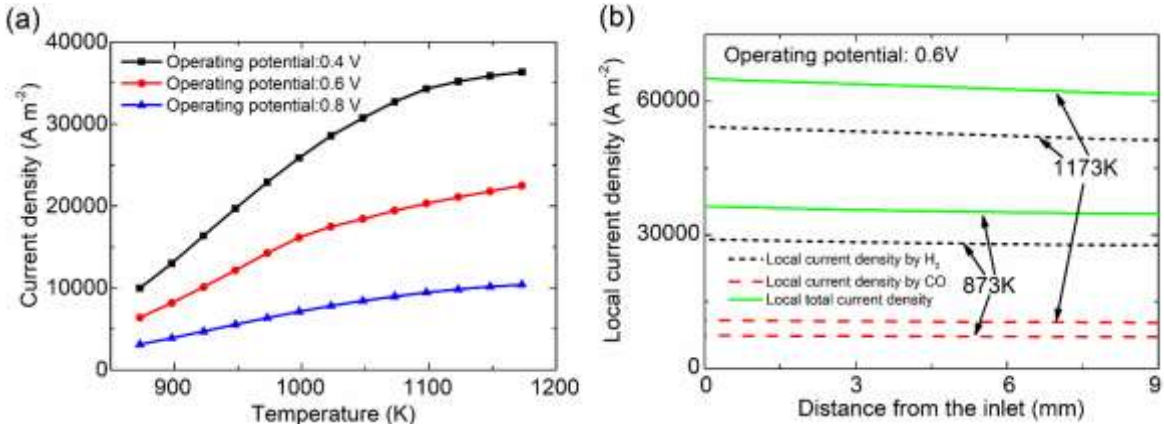

Figure 5 (a) The effect of temperature on the output current density at different operating potentials; (b) The current source distribution at the anode-electrolyte interface.

It is known that the temperature of inlet has a great positive effect on the both chemical reactions (MDR and WGSR) and electrochemical oxidations of the fuels (CO and H_2).

Simulations are conducted to explore the power output of the SOFC with the increase of temperatures from 873 K to 1173 K. The output current density of the SOFC fueled by pure methanol is shown in Figure 5a. As expected, the current densities are increased considerably with operating temperatures increasing. This phenomenon is mainly caused by the higher rate of methanol decomposition reaction (generating more CO and H_2) and faster water gas shift reaction kinetics (producing more H_2) at a higher operating temperature. Besides, a higher temperature can also benefit the ionic conduction of the electrolyte significantly and the rates of electrochemical reactions (generating more electrons per unit time), which can be proved by the current sources of the SOFC at the anode-electrolyte interface (Figure 5b).

In addition, the rates of MDR and WGSR are all increased with the increase of the temperature. Although the peak rates for MDR remain same for both two temperatures, the average rate of MDR in porous anode is increased from about 104 mol m^{-3} s^{-1} at 873 K to approximate 129 mol m^{-3} s^{-1} at 1173 K (Figure 6a,b). Moreover, for the WGSR, the rate is increased considerably as the temperature rises (Figure 6c,d), and the peak rate at 1173 K (60.4 mol m^{-3} s^{-1}) is much higher than that at 873 K (0.17 mol m^{-3} s^{-1}). The higher rates of MDR and WGSR at 1173 K tend to consume more CH_3OH and produce more H_2 and CO, which will increase the Nernst potentials caused by H_2 and CO fuels. Besides the higher temperature is likely to lower the ohmic overpotential losses because the oxygen ion conductivity of the electrolyte is sensitive to the temperature.[36] Therefore, a higher output current density can be obtained at a higher temperature because of the temperature effects on the Nernst potentials and the ohmic overpotential losses. Increased chemical reactions (MDR and WGSR) produce more hydrogen. On the other hand, the higher output current density definitely consumes more hydrogen. As a result, these combined effects cause the average molar fraction of hydrogen in the porous anode at 1173 K only slightly lower than that at 873 K (Figure 7a,b). However, more methanol is consumed due to the increased rate of MDR, causing larger drop in the average CH_3OH molar fraction in the anode when the temperature is increased to 1173 K (Figure 7c,d).

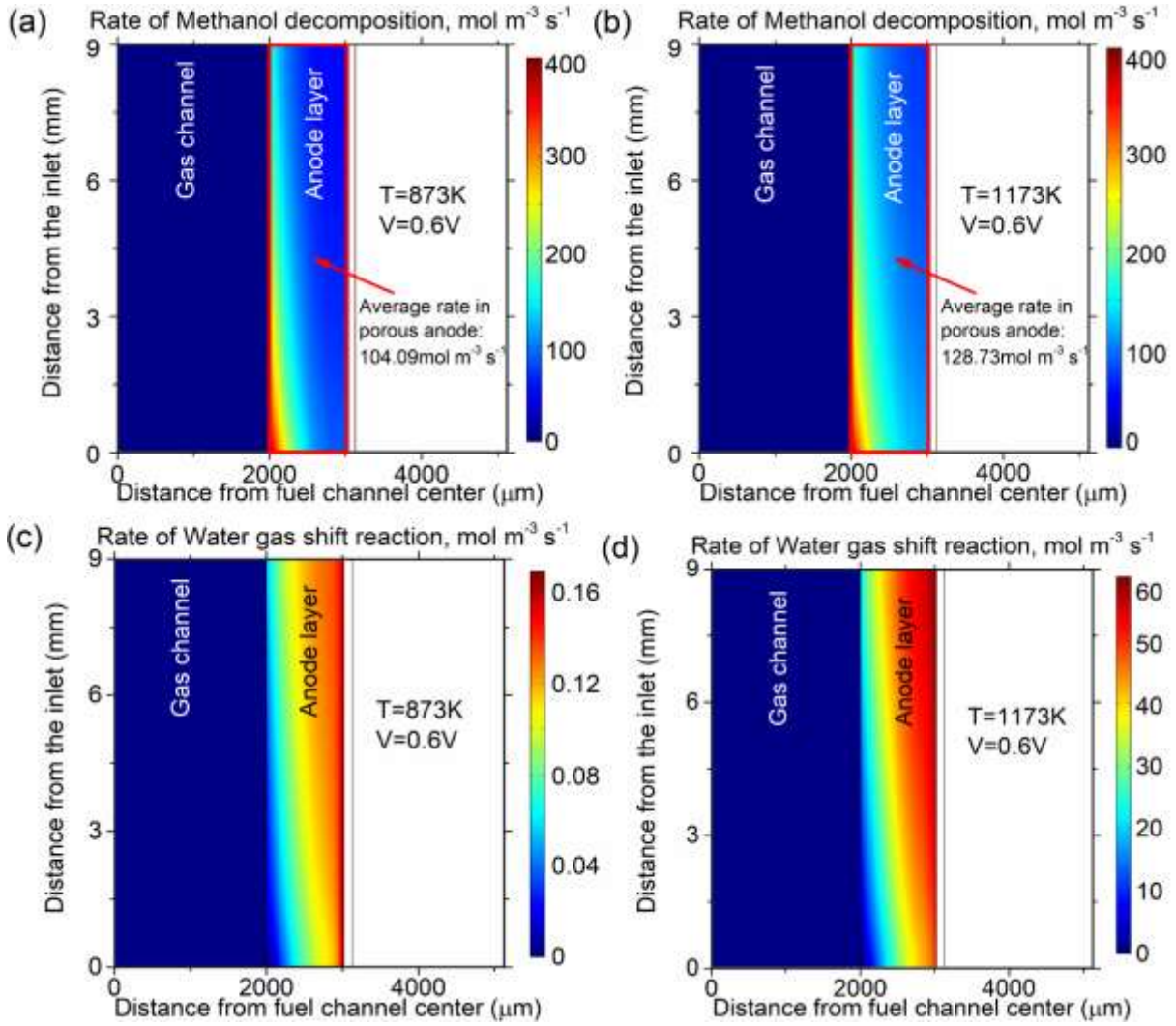

Figure 6 Reaction rate distributions at different temperatures: (a) MDR at 873 K; (b) MDR at 1173 K; (c) WGSR at 873 K; (d) WGSR at 1173 K.

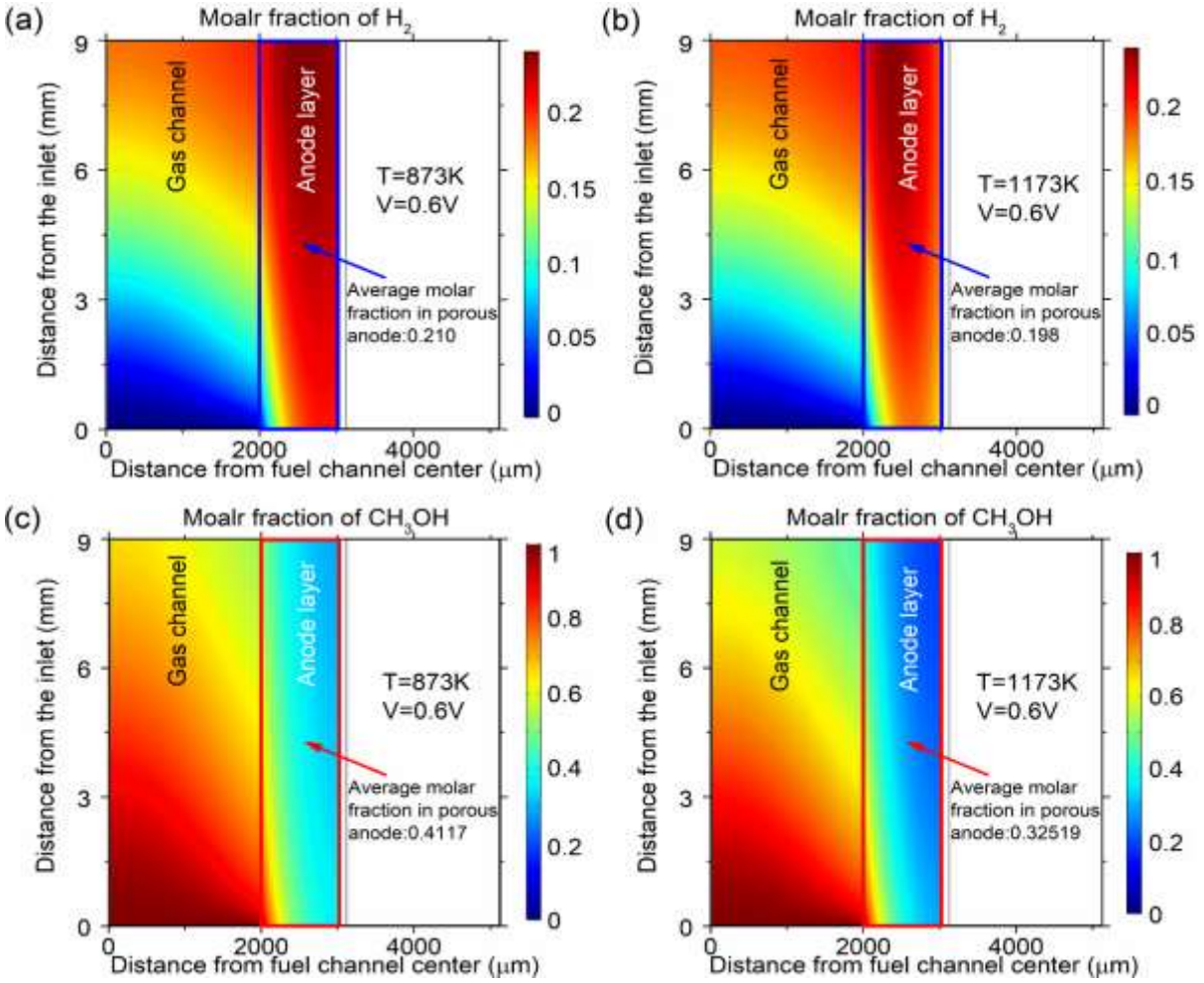

Figure 7 Species molar fractions at different temperatures: (a) H_2 at 873 K; (b) H_2 at 1173 K; (a) CH_3OH at 873 K; (b) CH_3OH at 1173 K.

3.3 The effect of the operating potential

Simulations are conducted at typical operating potentials (0.4 V, 0.6 V and 0.8 V), since the performance of an SOFC can be profoundly influenced by the operating potential. Output current densities are presented in Figure 5a. As expected, the output current density is increased significantly with the decrease of the operating potential, especially at higher temperature. In addition, current sources by both H_2 and CO fuels are highly enhanced at lower voltage, so does the total current source (Figure 8). Highly increased consumptions of H_2 and CO fuels by the electrochemical reactions lead to the more generations of the water and carbon dioxide at lower operating potential, which can be proved by the differences of molar fractions of water and carbon dioxide at different operating potentials. The peak molar fractions for CO_2 and H_2O are increased considerably from 0.0504 to 0.265 and from 0.116 to 0.498, respectively (Figure 9).

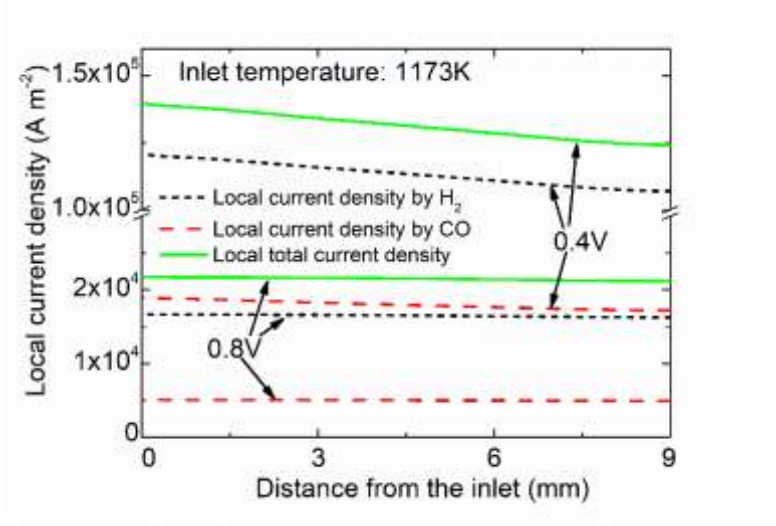

Figure 8 The current source distributions at the anode-electrolyte interface.

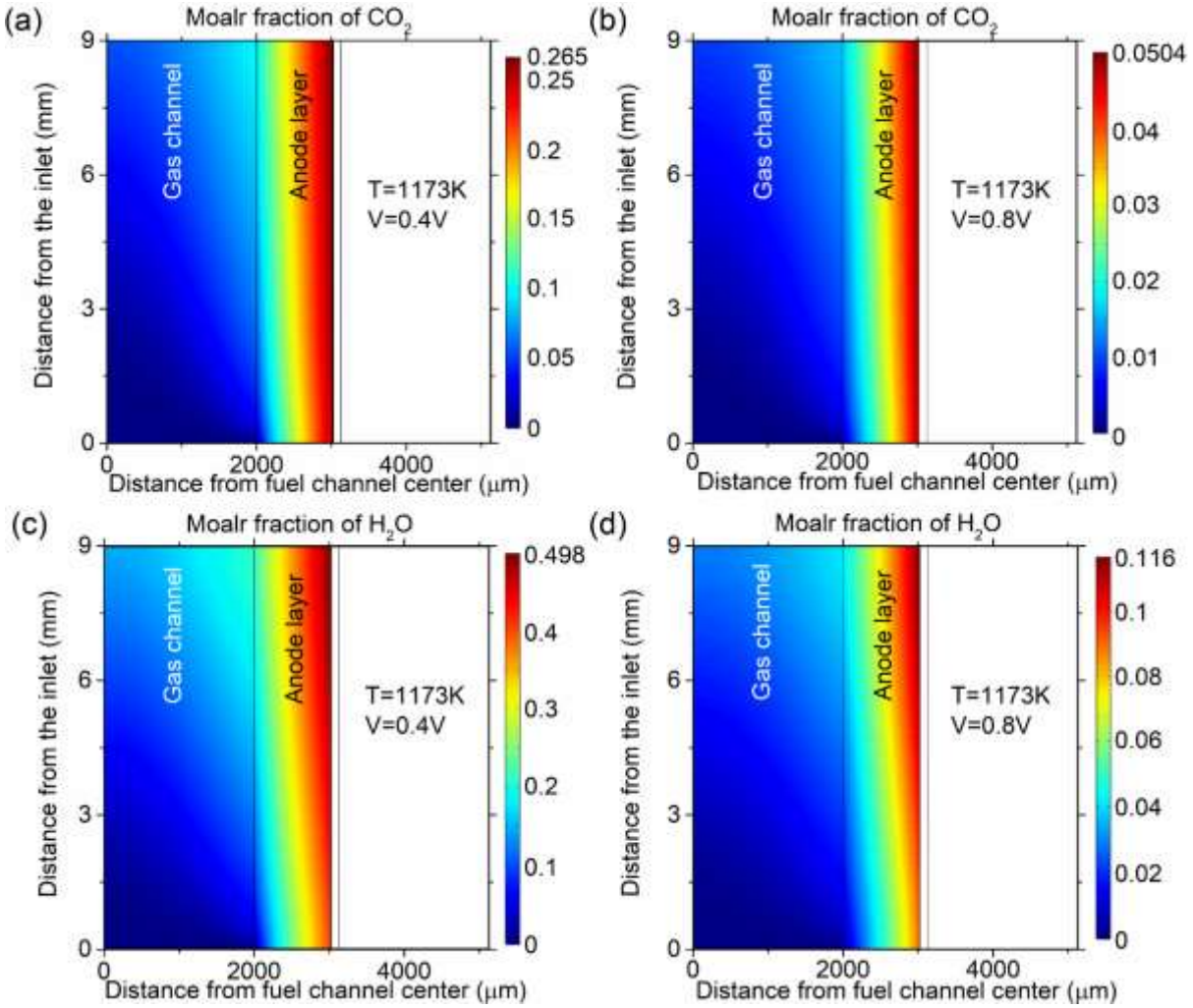

Figure 9 Molar fractions of CO_2 at: (a) 0.4 V; (b) 0.8 V; molar fractions of H_2O at: (c) 0.4 V; (d) 0.8 V.

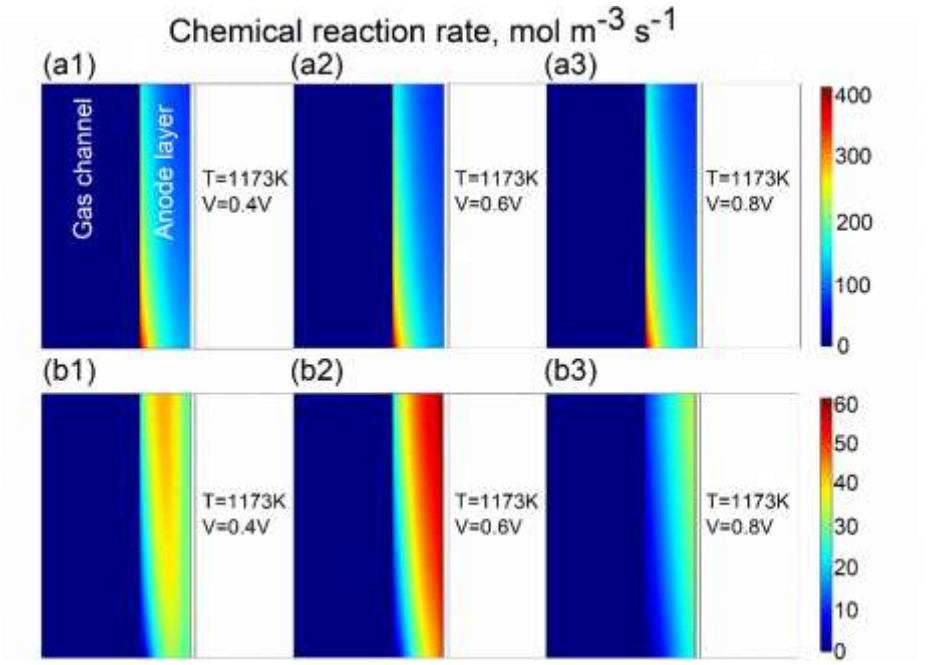

Figure 10 The reaction rate distributions at different potentials: (a1-a3) MDR; (b1-b3) WGSR.

The rate distributions of MDR and WGSR at three typical operating potentials (0.4 V 0.6 V 0.8 V) are also shown in Figure 10. It is obvious that the peak rates and rate distributions for MDR in these three situations almost remain same. For comparison, the WGSR rates are quite different as the operating potential increases from 0.4 V to 0.8 V, which is mainly caused by the gas composition variation in the cell (Figure 11). When the operating potential is 0.4 V, the higher output current density at lower potential tends to consume more CO and H_2 fuels, which favours the water gas shift reaction to generate H_2 but consume more CO as the hydrogen electrochemical oxidation is faster.[28] When the potential increases to 0.6 V, molar fraction of carbon monoxide is increased due to decreased current density. Besides, the consumption of the H_2 still benefits the water gas shift reaction despite lower current density. Therefore, the higher molar fraction of carbon monoxide at 0.6 V makes the rate of WGSR higher than the rate at 0.4 V. As the potential rises to 0.8 V, higher molar fraction of carbon monoxide, lower consumption of hydrogen and lower generation of water because of the lower current density cause the lower rate of WGSR.

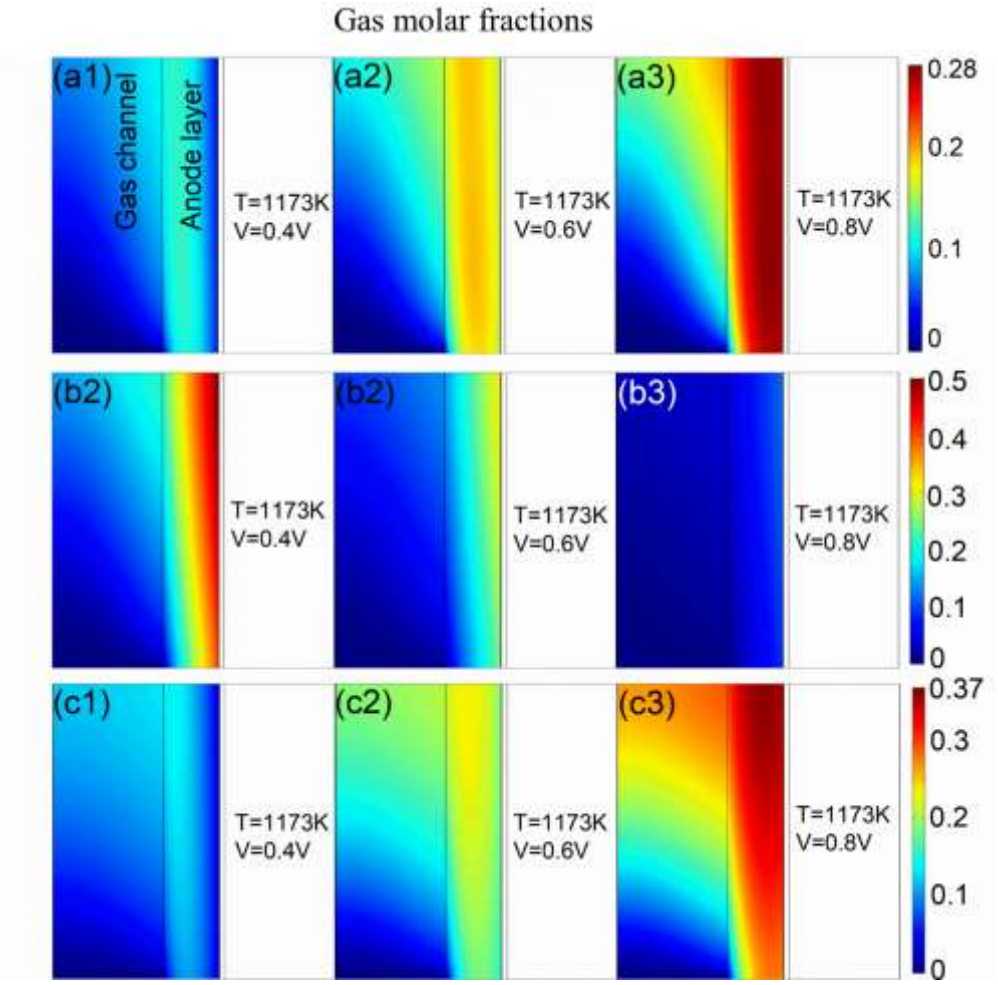

Figure 11 Gas compositions: (a1-a3) CO; (b1-b3) H_2O; (c1-c3) H_2.

3.4 The effect of the structural dimensions of the SOFC

In the SOFC, the length of the cell and the thickness of the anode are important structural parameters, because the longer length and thicker anode can provide more space for electrochemical/chemical reactions, which will affect the gas composition in the porous anode and the power output of the SOFC. Therefore, the simulation is conducted to investigate the effects of the cell length and the anode thickness on the SOFC performance and the methanol conversion at temperature of 1073 K and operating potential of 0.6 V.

The calculated output current density based on the different lengths is shown in Figure 12a. It can be observed that the current density is decreased slightly when the length of the cell is increased from 9 mm to 90 mm, which is mainly caused by the combined effects of the decreasing of CO and H_2 and the increasing of H_2O and CO_2 (Figure 12b). Figure 12b shows the methanol conversion and the molar fraction variations of the gases at the outlet of the fuel channel while the length varies. It obviously indicates that the conversion of the methanol is increased considerably at the beginning of the length increase and varies slightly when the length of SOFC exceeds 50 mm (reaches > 0.9 when the length is longer than 54 mm). Different

from the effect of the cell length on the current density, the thickness of the anode tends to benefit the performance of the SOFC. Figure 13a shows that the current density is increased with increasing anode thickness. However, as the anode thickness is over 800 μm, a further increase in anode thickness causes the SOFC performance to decrease slightly. This is because a thicker anode benefits methanol conversion for H_2 and CO production (Figure 13b) but a too thick anode will cause a high gas diffusion resistance. As a result, an optimal anode thickness between 600 μm and 800 μm is suggested for the present direct methanol SOFC model. The length of the cell and the thickness of the anode both benefit the methanol conversion, while they have different influences on the performance of the SOFC. The increasing of methanol conversion is due to more catalyst reaction sites, and the different effects on the current density are because of the different fuel concentrations.

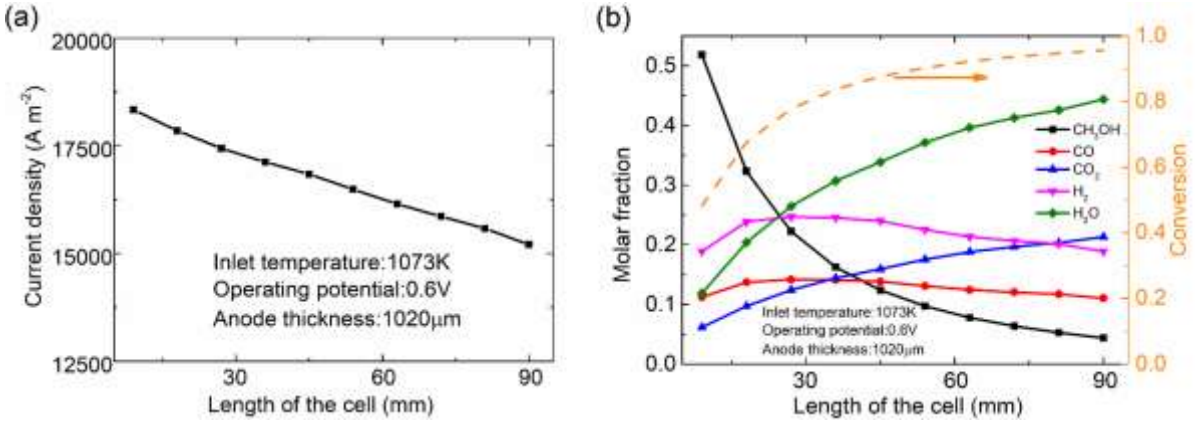

Figure 12 The effects of cell length on: (a) the output current density; (b) the CH_3OH conversion and gas composition at the outlet of the fuel channel.

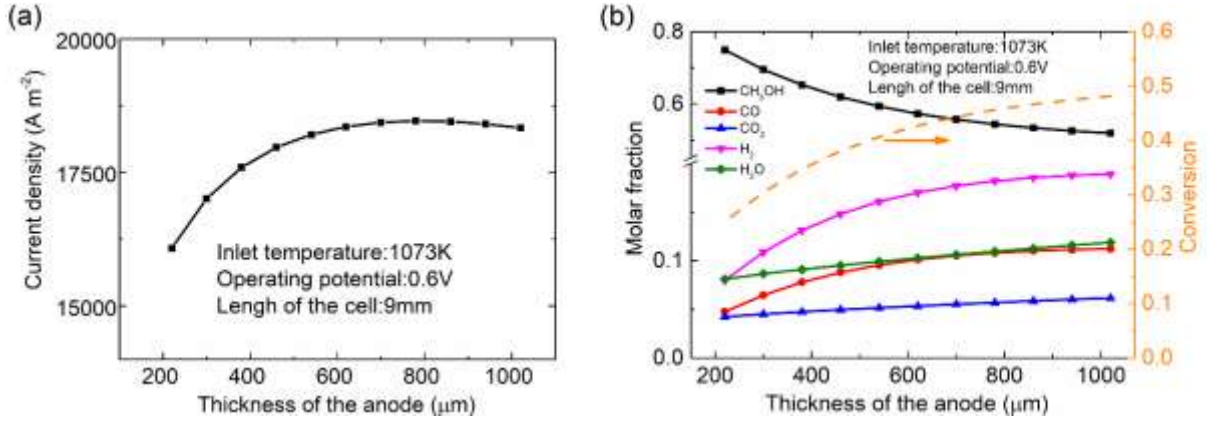

Figure 13 The effects of anode thickness on: (a) the output current density; (b) the CH_3OH conversion and gas composition at the outlet of the fuel channel.

4 Conclusions

A 2D mathematic model is developed to investigate the current-potential characteristic of the pure methanol-fueled SOFC with considering the MDR and WGSR in the catalytic anode layer.

Electrochemical/chemical reactions, electron/ion charge transports and fluid flow as well as the mass transfer in the cell are fully considered. Parametric simulations are conducted after model validation.

It is found that the rate of the MDR is the highest (405 mol m^{-3} s^{-1}) near the inlet and decreases along the anode, leading to the decrease of the methanol concentration along the fuel channel, while the WGSR rate is the highest (15.2 mol m^{-3} s^{-1}) in the downstream of the anode due to the reactant accumulation, which cause locally different distributions of the hydrogen and the carbon monoxide. The temperature of inlet can considerably affect the SOFC performance by facilitating the chemical and electrochemical reactions as well as the ion conduction. Because of the higher current density, more methanol is consumed at higher temperature. Current density and gas composition are all significantly influenced by the operating potential. Current density is decreased with increasing potential, and the fuels (hydrogen and carbon monoxide) tend to accumulate at the anode at high operating potential due to the low current density. Although thicker anode benefits the methanol conversion, the anode thickness should not be too high in order to avoid significant resistance for gas diffusion (600 μm - 800 μm is suggested for the present model). In addition, the current density of SOFC is found to decrease with increasing cell length. It is worth noting that because of the small cell size, the whole cell is considered as an isothermal domain in the present study. Due to the fact that the simultaneous endothermic methanol decomposition and the exothermic chemical/electrochemical reactions indeed complicate the temperature distribution of the cell, and the temperature gradient caused is an important factor for evaluating whether the SOFC could maintain a stable operation for a long period of time. Based on these considerations the heat transfer sub-model can be employed in the subsequent research.

The present study provides useful information to understand the mechanisms of the SOFC running on the pure methanol. Specific operating conditions and structural dimensions are found to improve the efficiency and the performance of SOFC.

Acknowledgments

M. Ni thanks the funding support (Project Number: PolyU 152214/17E and PolyU 152064/18E) from Research Grant Council, University Grants Committee, Hong Kong SAR.

References

1. Singhal SC, Kendall K. *High-Temperature Solid Oxide Fuel Cells: Fundamentals, Design and Applications*. Elsevier; 2003.
2. Zhao T, Kreuer K-D, Nguyen T Van. *Advances in Fuel Cells*. Elsevier; 2007.
3. Lin Y, Zhan Z, Liu J, Barnett SA. Direct operation of solid oxide fuel cells with methane fuel. *Solid State Ionics*. 2005;176(23-24):1827-1835.
4. Kaur G, Basu S. Physical characterization and electrochemical performance of copper-iron-ceria-YSZ anode-based SOFCs in H2 and methane fuels. *Int J Energy Res*. 2015;39(10):1345-1354.
5. Eguchi K, Kojo H, Takeguchi T, Kikuchi R, Sasaki K. Fuel flexibility in power generation by solid oxide fuel cells. *Solid State Ionics*. 2002;152-153:411-416.
6. Gao Z, Raza R, Zhu B, Mao Z. Development of methanol-fueled low-temperature solid oxide fuel cells. *Int J Energy Res*. 2011;35(8):690-696.
7. Fuerte A, Valenzuela RX, Escudero MJ, Daza L. Ammonia as efficient fuel for SOFC. *J Power Sources*. 2009;192(1):170-174.
8. Ni M, Leung DYC, Leung MKH. Mathematical modeling of ammonia-fed solid oxide fuel cells with different electrolytes. *Int J Hydrogen Energy*. 2008;33(20):5765-5772.
9.
9. Palo DR, Dagle RA, Holladay JD. Methanol steam reforming for hydrogen production. *Chem Rev*. 2007;107(10):3992-4021.
10. Gattrell M, Gupta N, Co A. Electrochemical reduction of CO2 to hydrocarbons to store renewable electrical energy and upgrade biogas. *Energy Convers Manag*. 2007;48(4):1255-1265.
11. Cimenti M, Hill JM. Direct utilization of liquid fuels in SOFC for portable applications: Challenges for the selection of alternative anodes. *Energies*. 2009;2(2):377-410.
12. Olah GA. Beyond oil and gas: The methanol economy. *Angew Chemie - Int Ed*. 2005;44(18):2636-2639.
13. Neelakandan S, Liu D, Wang L, Hu M, Wang L. Highly branched poly(arylene ether)/surface functionalized fullerene-based composite membrane electrolyte for DMFC applications. *Int J Energy Res*. 2019;43(8):3756-3767.
14. Munjewar SS, Thombre SB, Mallick RK. Approaches to overcome the barrier issues of passive direct methanol fuel cell – Review. *Renew Sustain Energy Rev*. 2017;67:1087-1104.
15. Neburchilov V, Martin J, Wang H, Zhang J. A review of polymer electrolyte

membranes for direct methanol fuel cells. *J Power Sources*. 2007;169(2):221-238.

16. Bresciani F, Casalegno A, Bonde JL, Odgaard M, Marchesi R. A comparison of operating strategies to reduce DMFC degradation. *Int J Energy Res*. 2014;38(1):117-124.
17. Jiang Y, Virkar A V. A High Performance, Anode-Supported Solid Oxide Fuel Cell Operating on Direct Alcohol. *J Electrochem Soc*. 2001;148(7):A706.
18. Liu M, Peng R, Dong D, Gao J, Liu X, Meng G. Direct liquid methanol-fueled solid oxide fuel cell. *J Power Sources*. 2008;185(1):188-192.
19. Meng X, Zhan Z, Liu X, Wu H, Wang S, Wen T. Low-temperature ceria-electrolyte solid oxide fuel cells for efficient methanol oxidation. *J Power Sources*. 2011;196(23):9961-9964.
20. Sasaki K, Watanabe K, Teraoka Y. Direct-Alcohol SOFCs: Current-Voltage Characteristics and Fuel Gas Compositions. *J Electrochem Soc*. 2004;151(7):A965.
21. Saunders GJ, Preece J, Kendall K. Formulating liquid hydrocarbon fuels for SOFCs. *J Power Sources*. 2004;131(1-2):23-26.
22. Shi Y, Li C, Cai N. Experimental characterization and mechanistic modeling of carbon monoxide fueled solid oxide fuel cell. *J Power Sources*. 2011;196(13):5526-5537.
23. Xu H, Chen B, Liu J, Ni M. Modeling of direct carbon solid oxide fuel cell for CO and electricity cogeneration. *Appl Energy*. 2016;178:353-362.
24. Laosiripojana N, Assabumrungrat S. Catalytic steam reforming of methane, methanol, and ethanol over Ni/YSZ: The possible use of these fuels in internal reforming SOFC. *J Power Sources*. 2007;163(2):943-951.
25. Lawlor V. Review of the micro-tubular solid oxide fuel cell (Part II: Cell design issues and research activities). *J Power Sources*. 2013;240:421-441.
26. Mizsey P, Newson E, Truong T binh, Hottinger P. The kinetics of methanol decomposition: A part of autothermal partial oxidation to produce hydrogen for fuel cells. *Appl Catal A Gen*. 2001;213(2):233-237.
27. Haberman BA, Young JB. Three-dimensional simulation of chemically reacting gas flows in the porous support structure of an integrated-planar solid oxide fuel cell. *Int J Heat Mass Transf*. 2004;47(17-18):3617-3629.
28. Ni M. Modeling and parametric simulations of solid oxide fuel cells with methane carbon dioxide reforming. *Energy Convers Manag*. 2013;70:116-129.
29. Matsuzaki Y, Yasuda I. Electrochemical oxidation of H2 and CO in a H2-H2O-CO-CO2 system at the interface of a Ni-YSZ cermet electrode and YSZ electrolyte. *J*

Electrochem Soc. 2000;147(5):1630-1635.

30. Coker AK. Ludwig's Applied Process Design for Chemical and Petrochemical Plants. *gulf Prof Publ*. Published online 2007.
31. Krishna R, Wesselingh JA. The Maxwell-Stefan approach to mass tranfer. *Chem Eng Sci*. 1997;52(6):861-911.
32. Vural Y, Ma L, Ingham DB, Pourkashanian M. Comparison of the multicomponent mass transfer models for the prediction of the concentration overpotential for solid oxide fuel cell anodes. *J Power Sources*. 2010;195(15):4893-4904.
33. Evans RB, Watson GM, Mason EA. Gaseous diffusion in porous media at uniform pressure. *J Chem Phys*. 1961;35(6):2076-2083.
34. Veldsink JW, van Damme RMJ, Versteeg GF, van Swaaij WPM. The use of the dusty-gas model for the description of mass transport with chemical reaction in porous media. *Chem Eng J Biochem Eng J*. 1995;57(2):115-125.
35. Poling BE, Prausnitz JM, O'Connell JP. *The Properties of Gases and Liquids.*; 2001.
36. Ni M, Leung MKH, Leung DYC. Parametric study of solid oxide fuel cell performance. *Energy Convers Manag*. 2007;48(5):1525-1535.